Journal of Alloys and Compounds 513 (2012) 6–9

Contents lists available at SciVerse ScienceDirect

Journal of Alloys and Compounds

journal homepage: www.elsevier.com/locate/jallcom

Letter

Indium flux, growth temperature and RF power induced effects in InN layers grown on GaN/Si substrate by plasma-assisted MBE

Mahesh Kumar[a,b], Thirumaleshwara N. Bhat[a], Mohana K. Rajpalke[a], Basanta Roul[a,b], A.T. Kalghatgi[b], S.B. Krupanidhi[a,*]

[a] Materials Research Centre, Indian Institute of Science, Bangalore 560012, India
[b] Central Research Laboratory, Bharat Electronics, Bangalore 560013, India

ARTICLE INFO

Article history:
Received 17 August 2011
Received in revised form
30 September 2011
Accepted 3 October 2011
Available online 17 October 2011

Keywords:
Indium nitride
MBE
X-ray diffraction
Luminescence

ABSTRACT

In the present work, we report the growth of wurtzite InN epilayers on GaN/Si (1 1 1) substrate by plasma-assisted molecular beam epitaxy (PAMBE). The growth parameters such as indium flux, substrate temperature and RF power affect the crystallographic and morphological properties of InN layers, which were evaluated using high resolution X-ray diffraction (HRXRD) analysis and atomic force microscopy (AFM). It is found that excess indium (In) concentrations and surface roughness were increased with increase in In flux and growth temperature. The intensity of HRXRD (0 0 0 2) peak, corresponding to *c*-axis orientation has been increased and full width at half maxima (FWHM) has decreased with increase in RF power. It was found that highly *c*-axis oriented InN epilayers can be grown at 450 °C growth temperature, 450 W RF power and 1.30×10^{-7} mbar In beam equivalent pressure (BEP). The energy gap of InN layers grown by optimizing growth conditions was determined by photoluminescence and optical absorption measurement.

1. Introduction

Indium nitride (InN) epitaxial layers and devices are currently under intense investigation, mainly due to the material's promising properties such as small effective mass, high electron drift velocity, and small band gap energy [1,2], which make it ideal for fast electronic devices, high efficiency solar cells and infrared laser diodes [3,4]. This narrow bandgap allows the group III-nitrides alloy system, such as (AlGaIn)N-based light emission devices, the possibility to operate in an extremely wide wavelength range from near-infrared to deep ultraviolet (0.7–6.2 eV). Initially, the InN films have been deposited by sputtering techniques, in which oxygen incorporation is a severe problem and the optical absorption was predominantly found at around 1.9 eV [5]. In contrast, the InN films grown by molecular-beam epitaxy (MBE) and metalorganic vapor phase epitaxy (MOVPE) techniques show much narrower direct bandgap as well as a significant improvement of the crystalline quality. However, in growing pure InN layers, the main difficulty lies with its thermal decomposition, which becomes excessive above 500 °C and its impurity incorporation problem, especially by oxygen [6]. Plasma-assisted molecular beam epitaxy (PAMBE) is a suitable method for producing InN, because low growth temperatures are possible in combination with an ultra high vacuum (UHV) growth environment, thus reducing the impurity incorporation [7]. The variations in the band-gap measurements were mainly attributed to the Burstein–Moss energy shift [8], the presence of oxide precipitates [9,10], the formation of indium (In) clusters [11] and other stoichiometry-related defects [12].

In this paper, we have studied the effect of growth parameters such as indium flux, substrate temperature and RF power on the crystallographic and morphological properties of InN layers. The energy gap of InN layers grown by optimizing growth conditions was determined by photoluminescence (PL) and optical absorption measurement.

2. Experimental details

The samples used for this study were grown by PAMBE system equipped with a radio frequency plasma source. The undoped Si (1 1 1) substrates were chemically cleaned followed by dipping in 5% HF to remove the surface native oxide. The substrates were thermally cleaned at 900 °C for 1 h in ultra-high vacuum. In all samples, first we have grown ultrathin layer of β-Si_3N_4 on Si (1 1 1) surface by exposing the surface to RF nitrogen plasma with a high content of nitrogen atoms. Then, a low temperature GaN buffer layer of thickness ~20 nm was grown at 500 °C followed by ~225 nm of GaN epilayers at 700 °C and details of growth conditions can be found elsewhere [13]. Afterwards, in samples (a), (b) and (c), the LT-InN buffer layers of thickness 30 nm were grown at 400 °C followed by 250 nm of InN films at 450 °C and indium (In) beam equivalent pressure (BEP) was kept at 3.45×10^{-7}, 2.20×10^{-7}, and 1.30×10^{-7} mbar, respectively. Nitrogen flow rate and plasma power were kept constant at 0.5 sccm and 350 W. In samples (d) and (e), the LT-InN buffer layers of thickness 30 nm were grown at 400 °C followed by 250 nm of InN films at 500 °C and

* Corresponding author.
E-mail address: sbk@mrc.iisc.ernet.in (S.B. Krupanidhi).

0925-8388/$ – see front matter © 2011 Elsevier B.V. All rights reserved.
doi:10.1016/j.jallcom.2011.10.009

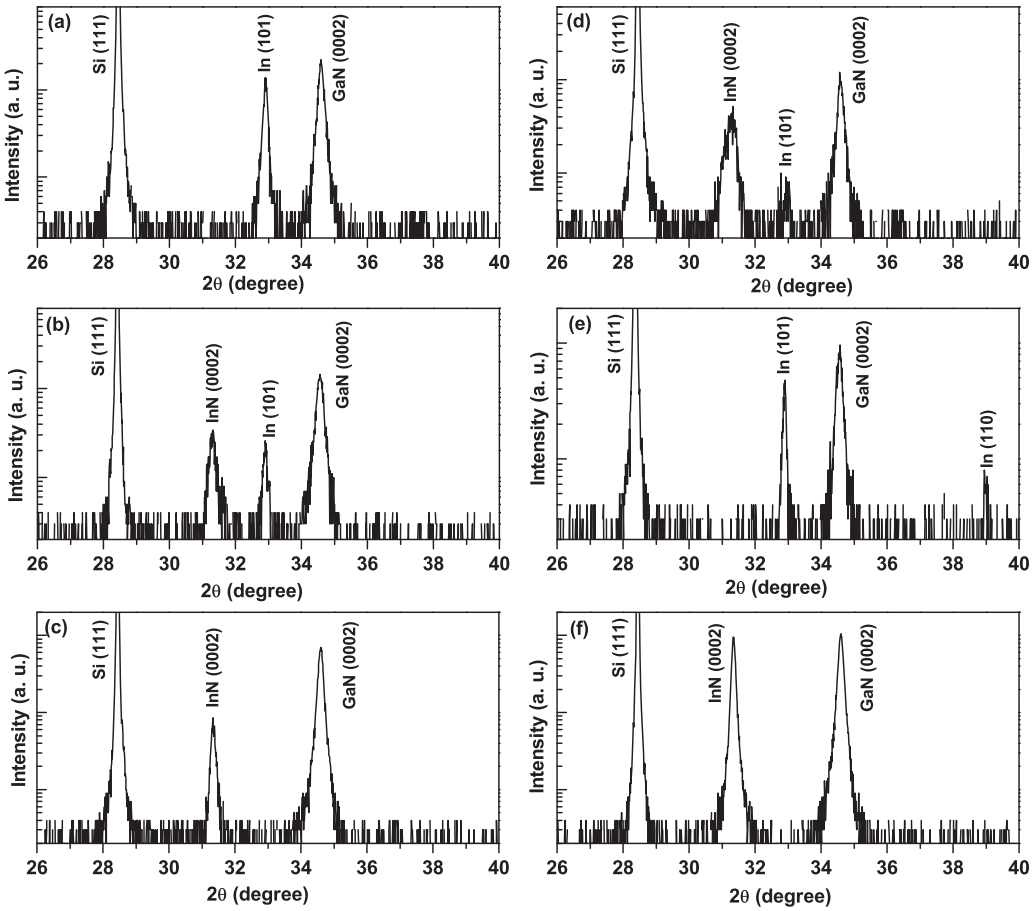

Fig. 1. (a)–(f) HRXRD 2θ–ω scans of InN heteroepitaxial layers of sample (a)–(f), grown on GaN/Si (1 1 1).

525 °C, respectively. The In BEP, nitrogen flow rate and plasma power were kept constant at 1.30×10^{-7} mbar, 0.5 sccm and 350 W as shown in Table 1. In sample (f), the LT-InN buffer layers of thickness 30 nm were grown at 400 °C followed by 250 nm of InN films at 450 °C. The In BEP, nitrogen flow rate and plasma power were kept at 1.30×10^{-7} mbar, 0.5 sccm and 450 W. The structural characterization and surface morphologies of the samples were carried out by high resolution X-ray diffraction (HRXRD) and atomic force microscopy (AFM), respectively. HRXRD measurements were carried out using a double crystal four-circle diffractometer (Bruker-D8 DISCOVER). AFM measurements were carried out using a VECCO (CP II) system. The PL spectra were recorded at 10 K using a closed cycle optical cryostat and He–Cd laser of 325 nm excitation wavelength with a maximum input power of 30 mW and optical absorption spectra were measured at room temperature for sample (f) by Bruker IFS 66v/s vaccum Fourier transform interferometer.

3. Result and discussion

Fig. 1(a)–(f) shows a typical 2θ–ω HRXRD scans of InN heteroepitaxial layers of sample (a)–(f), respectively. The peaks at $2\theta = 28.45°$, 31.33°, 32.95°, 34.58° and 39.03° are assigned to the Si (1 1 1), InN (0 0 0 2), In (1 0 1), GaN (0 0 0 2) and In (1 1 0) planes, respectively. From the figure it can be seen that the HRXRD diffraction intensities of InN layers decreased, when the In BEP was

Table 1
Growth parameters of InN layers grown on GaN/Si (1 1 1) substrate.

Sample name	In BEP (mbar)	Growth temp. (°C)	RF power (W)
(a)	3.45×10^{-7}	450	350
(b)	2.20×10^{-7}	450	350
(c)	1.30×10^{-7}	450	350
(d)	1.30×10^{-7}	500	350
(e)	1.30×10^{-7}	525	350
(f)	1.30×10^{-7}	450	450

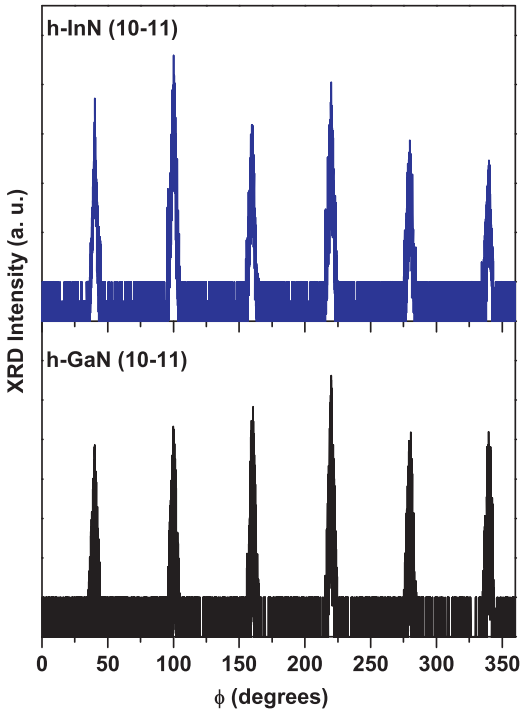

Fig. 2. In-plane Phi-scan measured from InN and GaN epilayers showing a sixfold symmetry.

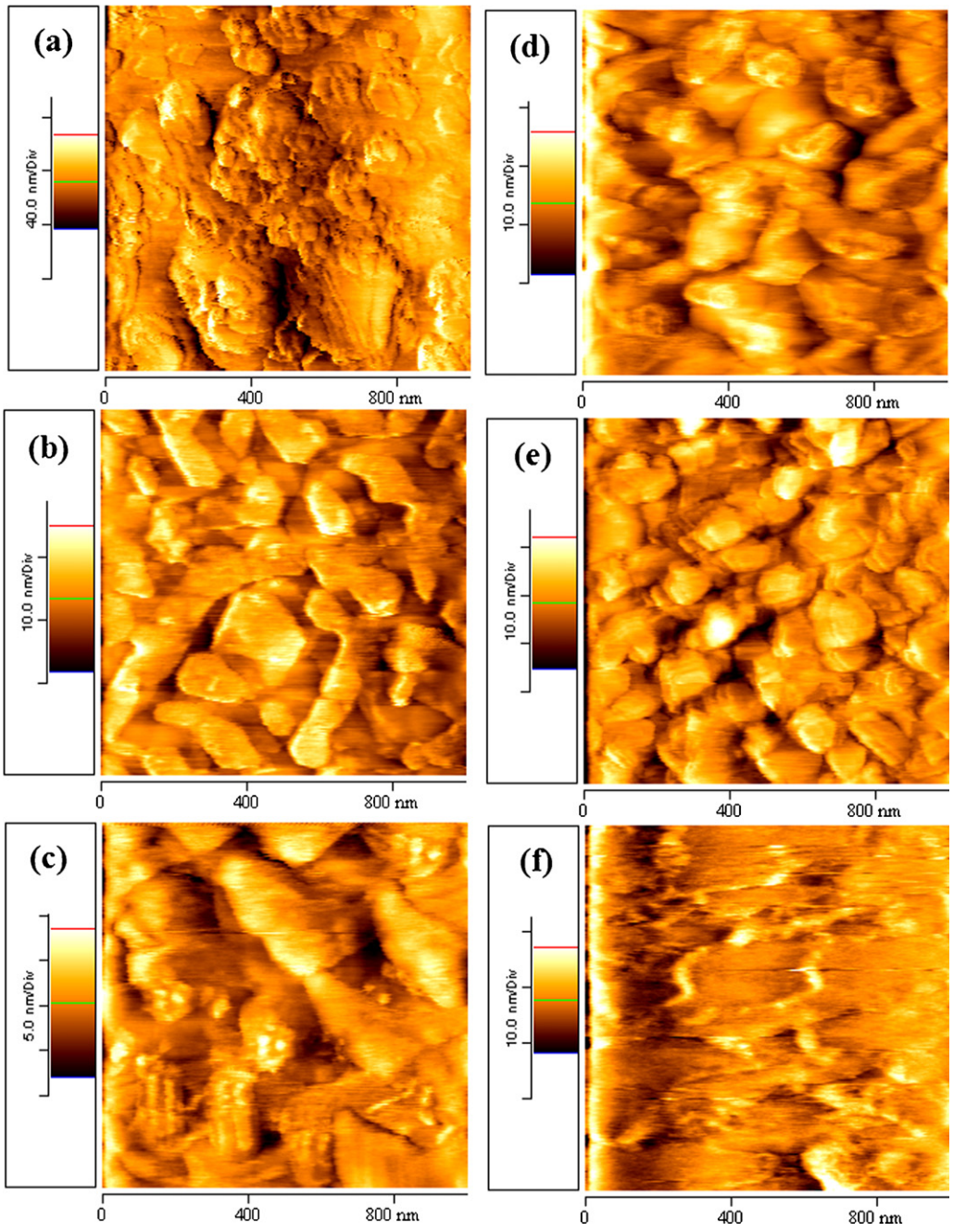

Fig. 3. (a)–(f) 1 μm × 1 μm AFM images of InN layers for sample (a)–(f), respectively.

increased from 1.30×10^{-7} to 2.20×10^{-7} mbar and also a In (1 0 1) peak has appeared at higher BEP. Further, increase in In BEP to 3.45×10^{-7} mbar, the InN (0 0 0 2) peak has completely disappeared and only In (1 0 1) peak has observed. In samples (c)–(e), the growth temperature varied from 450 °C to 525 °C and other parameters were kept constant. The InN (0 0 0 2) and In (1 0 1) phases was observed in sample (d), which was grown at 500 °C. In sample (e) only In peaks were observed, which was grown at 525 °C. In samples (c) and (f), the RF power varied and other parameters were kept constant. From Fig. 1(c) and (f), it can be seen that the HRXRD intensities of InN layers increased and full width at half maxima (FWHM) of (0 0 0 2) InN reflection of 2θ–ω scan has decreased with increase in RF power from 350 to 450 W. The X-ray rocking curve (XRC) of the (0 0 0 2) InN reflection of sample (f) was measured and the FWHM was found to be ~19″. An in-plane Phi scan was also taken by rotating the sample around its surface-normal direction to investigate the in-plane alignment between InN epilayers and under lying GaN epilayers. The Phi scans of the InN (1 0 $\bar{1}$ 1) and GaN (1 0 $\bar{1}$ 1) peaks are presented in Fig. 2. The hexagonal structure of InN produces six equal-spaced peaks. The absence of any other random peaks suggests that the InN film grains predominantly grow in the direction of [0 0 0 1], and the 0° shift between the InN and GaN is explained by coherent in-plane growth.

Table 2
The RMS roughness of the InN layers grown at different growth parameters.

Sample name	(a)	(b)	(c)	(d)	(e)	(f)
RMS roughness (nm)	11.67	3.93	2.77	4.07	4.62	3.18

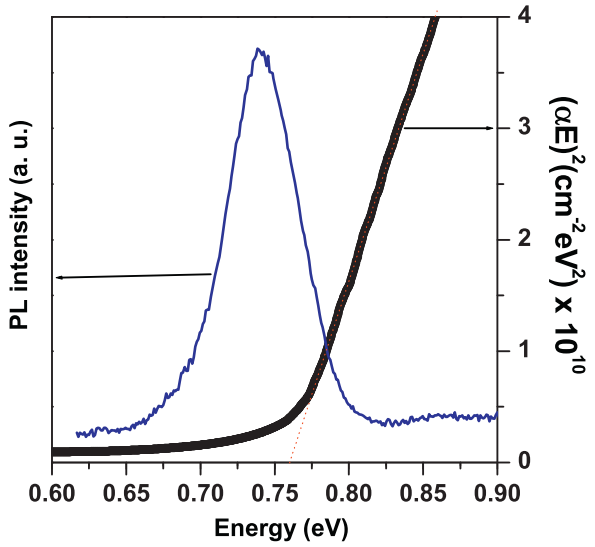

Fig. 4. PL and absorption spectra of InN layers (sample (f)). Solid lines are extrapolations to the energy axis (dotted lines) to determine the absorption edges.

Fig. 3(a)–(f) shows 1 μm × 1 μm AFM images of the InN layers for samples (a)–(f), respectively. The simplest and most common method used for the observation of changes in surface topography is called the root mean square (RMS) roughness calculation (σ). This roughness calculation is based on finding a median surface level for the image and then evaluating the standard deviation within the image. The equation for determining the surface roughness is [14].

$$\sigma = \sqrt{\frac{1}{N^2}\sum_{i=1}^{N}\sum_{j=1}^{N}\left(H(i,j)-\bar{H}\right)^2} \quad (1)$$

where i and j are the pixel locations on the AFM image, $\bar{H}$ is the mean height of the surface and $H(i,j)$ is the height of the surface at locations i and j, and N is the number of data points in the image. The RMS roughness of the InN layers has been calculated by using Image Analysis (IP 2.1) software from 1 μm × 1 μm AFM images and shown in Table 2. It can be seen from the table that the RMS roughness of the InN layers drastically decreased from 11.67 to 2.77 nm when the In flux has been decreased from 3.45×10^{-7} to 1.30×10^{-7} mbar. The RMS roughness of the InN layers increases with In flux due to the excess In with InN layers. When the growth temperature increases from 450 to 525 °C, RMS roughness of the InN layers increases, reflecting the transition from two-dimensional like growth mode to three-dimensional growth mode. The RMS roughness of the InN layers increases with increasing growth temperature due to InN dissociation and thus led to poor crystal quality accompanied by indium droplet formation. The RMS roughness of the InN layers slightly increases from 2.77 to 3.18 nm with RF power from 350 to 450 W. The higher RF power slightly increases the RMS roughness due to high energy nitrogen atoms but improve the crystalline quality of InN layers.

The optical properties of sample (f) were determined by photoluminescence (PL) and optical absorption measurement. Fig. 4 shows the PL and the absorption spectra of the InN layers (sample (f)). The PL were measured at 10 K and shows a strong band-edge emission peak around ~0.74 eV. The nature of the optical interband transition and value of the energy gap E_g can be determined using the relation derived independently by Tauc et al. [15] as $\alpha(E)E = A(E - E_g)^m$, where $m = 1/2$ for direct transitions and $m = 2$ for indirect transitions respectively. A is a disorder parameter nearly independent of the photon energy E. E_g is approximately taken as the energy band gap. Thus the value of the optical band gap for InN is obtained by plotting $(\alpha E)^2$ versus E in the high absorption range followed by extrapolating the linear region of the plots to $(\alpha E)^2 = 0$. The analysis of our data shows that the plots of $(\alpha E)^2$ versus E gives a linear relation. This indicates that the nature of the fundamental interband transition in InN layers is directly allowed. The optical band gap of InN is measured around ~0.76 and is shown by the dashed line in Fig. 4, which clearly demonstrates the characteristic feature of direct band gap absorption. According to Wu et al. [16] the band edge absorption energy depends on the carrier concentration and may not coincide with the PL peak energy. The absorption and PL measurement of band gap results in our work are ~0.76 and 0.74 eV, respectively. In recent literature, the optical band gap values are reported from 0.65 to 0.85 eV by different research groups [17,18]. It is found that blueshift of absorption edge can be induced by background electron concentration, and the higher electron concentration brings the larger blueshift, due to a possible Burstein–Moss effect.

4. Conclusion

The InN epilayers were grown on GaN/Si (1 1 1) substrate by PAMBE. The growth parameters such as indium flux, substrate temperature and RF power affect the crystallographic and morphological properties of InN layers. It is found that excess indium concentrations and surface roughness were increased with increase in In flux and growth temperature. The FWHM of HRXRD (0 0 0 2) peak has decreased with increase in RF power but also the RMS roughness has been increased slightly. The highly c-axis oriented InN epilayers can be grown at 450 °C substrate temperature, 450 W RF power and 1.30×10^{-7} mbar BEP of In. The energy gap of InN layers was determined by PL and optical absorption measurement and found to be ~0.74 and 0.76 eV.

References

[1] B.E. Foutz, S.K. O'Leary, M.S. Shur, L.F. Eastman, J. Appl. Phys. 85 (1999) 7727.
[2] J. Wu, W. Walukiewicz, K.M. Yu, J.W. Ager III, E.E. Haller, H. Lu, W.J. Schaff, Y. Saito, Y. Nanishi, Appl. Phys. Lett. 80 (2002) 3967.
[3] R. Ascazubi, I. Wilke, K. Denniston, H. Lu, W.J. Schaff, Appl. Phys. Lett. 84 (2004) 4810.
[4] C.J. Neufeld, N.G. Toledo, S.C. Cruz, M. Iza, S.P. DenBaars, U.K. Mishra, Appl. Phys. Lett. 93 (2008) 143502.
[5] Q.X. Guo, T. Tanaka, M. Nishio, H. Ogawa, X.D. Pu, W.Z. Shen, Appl. Phys. Lett. 86 (2005) 231913.
[6] X. Wang, A. Yoshikawa, Prog. Cryst. Growth Charact. Mater. 48/49 (2004) 42.
[7] Y. Nanishi, Y. Saito, T. Yamaguchi, Jap. J. Appl. Phys. 42 (2003) 2549.
[8] J. Wu, W. Walukiewicz, W. Shan, K.M. Yu, J.W. Ager, E.E. Haller, L. Hai, W.J. Schaff, Phys. Rev. B 66 (2002) 201403.
[9] D. Alexandrov, K. Scott, A. Butcher, M. Wintrebert-Fouquet, J. Vac. Sci. Technol. A 22 (2004) 954.
[10] M. Yoshimoto, H. Yamamoto, H. Wei, H. Harima, J. Saraie, A. Chayahara, Y. Horino, Appl. Phys. Lett. 83 (2003) 3480.
[11] J.C. Ho, P. Specht, Q. Yang, X. Xu, D. Hao, E.R. Weber, J. Appl. Phys. 98 (2005) 093712.
[12] K.S.A. Butcher, M. Wintrebert-Fouquet, P.P.T. Chen, T.L. Tansley, H. Dou, S.K. Shrestha, H. Timmers, M. Kuball, K.E. Prince, J.E. Bradby, J. Appl. Phys. 95 (2004) 6124.
[13] M. Kumar, B. Roul, T.N. Bhat, M.K. Rajpalke, P. Misra, L.M. Kukreja, N. Sinha, A.T. Kalghatgi, S.B. Krupanidhi, Mater. Res. Bull. 45 (2010) 1581.
[14] J.D. Kiely, D.A. Bonnell, J. Vacuum Sci. Technol. B 15 (1997) 1483.
[15] J. Tauc, R. Grigorovici, A. Vancu, Phys. Status Solidi 15 (1966) 627.
[16] J. Wu, W. Walukiewicz, W. Shan, K.M. Yu, J.W. Ager III, S.X. Li, E.E. Haller, H. Lu, W.J. Schaff, J. Appl. Phys. 94 (2003) 4457.
[17] A.G. Bhuiyan, A. Hashimoto, A. Yamamoto, J. Appl. Phys. 94 (2003) 2779.
[18] S. Gwo, C.L. Wu, C.H. Shen, W.H. Chang, T.M. Hsu, J.S. Wang, J.T. Hsu, Appl. Phys. Lett. 84 (2004) 3765.